Mechanistic Insights into the Light-Driven Catalysis of an Immobilized Lipase on Plasmonic Nanomaterials

ACS Catalysis

pubs.acs.org/acscatalysis Research Article

Mechanistic Insights into the Light-Driven Catalysis of an Immobilized Lipase on Plasmonic Nanomaterials

Heloise Ribeiro de Barros,* Isabel García, Christian Kuttner, Nicoll Zeballos, Pedro H. C. Camargo, Susana Inés Cordoba de Torresi, Fernando López-Gallego,* and Luis M. Liz-Marzán

Cite This: *ACS Catal.* 2021, 11, 414−423 Read Online

ACCESS | Metrics & More | Article Recommendations | Supporting Information

ABSTRACT: The use of light as an external stimulus to control the enzyme activity is an emerging strategy that enables accurate, remote, and noninvasive biotransformations. In this context, immobilization of enzymes on plasmonic nanoparticles offers an opportunity to create light-responsive biocatalytic materials. Nevertheless, a fundamental and mechanistic understanding of the effects of localized surface plasmon resonance (LSPR) excitation on enzyme regulation remains elusive. We herein investigate the plasmonic effects on biocatalysis using Au nanospheres (AuNSp) and nanostars (AuNSt) as model plasmonic nanoparticles, lipase from *Candida antarctica* fraction B (CALB) as a proof-of-concept enzyme, and 808 nm as near-infrared light excitation. Our data show that LSPR excitation enables an enhancement of 58% in the enzyme activity for CALB adsorbed on AuNSt, compared with the dark conditions. This work shows how photothermal heating over the LSPR excitation enhances the CALB activity through favoring product release in the last step of the enzyme mechanism. We propose that the results reported herein shed important mechanistic and kinetic insights into the field of plasmonic biocatalysis and may inspire the rational development of plasmonic nanomaterial−enzyme hybrids with tailored activities under external light irradiation.

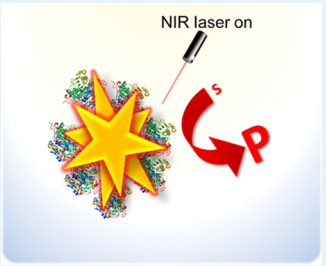

KEYWORDS: *biocatalysis, gold nanostructures, LSPR-enhanced mechanisms, nanotechnology, plasmonic heating, triggered bioactivity*

INTRODUCTION

Plasmonic nanomaterials, such as gold nanoparticles (Au NPs), display remarkable optical properties in the visible and near-infrared (NIR) spectral regions.[1−3] Such properties arise as a result of the excitation of localized surface plasmon resonances (LSPRs). It has been established that LSPR excitation in plasmonic NPs can accelerate a myriad of chemical transformations.[4−7] This catalytic effect can occur as a result of the generation of LSPR-excited charge carriers (hot electrons and hot holes) and/or photothermal heating following plasmon decay.[4,8,9] Surprisingly, only a few studies have explored the use of LSPR excitation to tune biocatalytic reactions.[10−15]

The conjugation of enzymes to plasmonic NPs is attractive for applications in biomedicine, such as photothermal therapy[16,17] and bioimaging,[18] as well as in chemical manufacturing.[13] In fact, the use of plasmonic effects at the interface between nanoparticles and enzymes is gaining momentum as a tool to remotely control biocatalytic processes using light as an external stimulus.[12,13,19] This field, plasmonic biocatalysis, paves the way to tuning enzyme properties in a noninvasive manner, enabling spatiotemporal control over the biocatalytic processes.[12,13] Despite these fascinating opportunities, the mechanisms at the "nano−bio" interface underlying the influence of plasmonic effects on enzyme functionality are poorly understood.[10,12,20]

What is already known is that the enzyme/nanomaterial interface plays an important role in the transport of substrates and products from the bulk to the enzyme active site, and vice versa, thereby altering the enzyme activity.[21] For example, recent insightful mechanistic studies revealed that the conjugation of hydrolases (i.e., phosphotriesterase) to quantum dots and Au NPs enhances the enzymatic kinetic efficiency, compared to their free counterparts.[22,23] Furthermore, kinetic studies under high-viscosity conditions demonstrate that the increase in the apparent catalytic rate (k_{cat}) relies on higher product-release kinetic constants associated with the last step of the hydrolase catalytic mechanism. Nevertheless, how those kinetic parameters may be altered by light at the interface between the enzyme and plasmonic nanomaterials is still an open question that remains largely underexplored.

To bridge this gap, we herein report a detailed and systematic study of the effects of LSPR excitation on the activity and enhancement mechanisms in plasmonic biocatalysis. In particular, we selected the lipase from *Candida antarctica* fraction B (CALB) as a proof-of-concept enzyme, whose catalytic mechanism is well understood, Au nanospheres (AuNSp) and nanostars (AuNSt) as model plasmonic NPs,

Received: November 11, 2020
Revised: December 9, 2020
Published: December 21, 2020

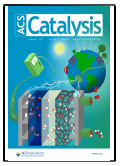

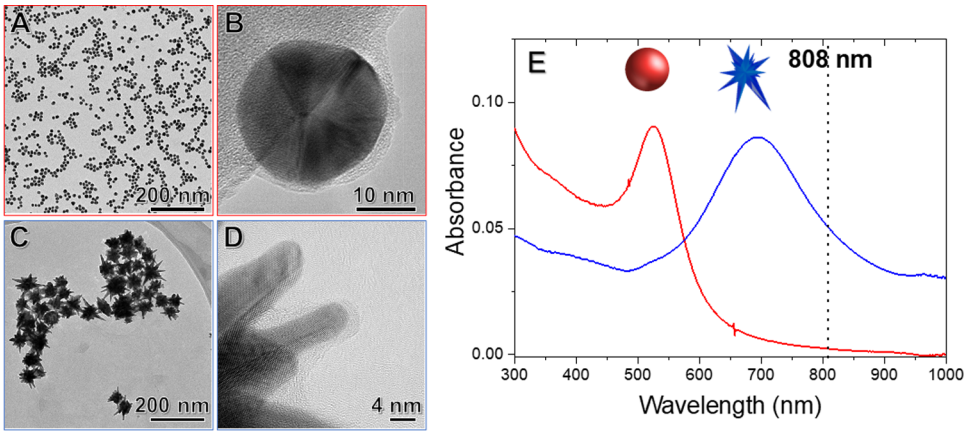

Figure 1. (A-D) TEM (A and C) and high-resolution TEM (B and D) images of AuNSp@CALB (A and B) and AuNSt@CALB (C and D). (E) UV−vis extinction spectra recorded from aqueous suspensions containing AuNSp@CALB (red trace) and AuNSt@CALB (blue trace). The 808 nm wavelength employed for biocatalysis studies is indicated by a black dashed line.

and an NIR laser as the light excitation source. Both on- (AuNSt) and off- (AuNSp) resonance conditions relative to the NIR laser source were investigated to demonstrate the LSPR-driven enhancement effects. Although CALB has been previously conjugated to Au NPs,[24−26] control over its catalytic activity through plasmonic effects remains elusive. Our data suggest that the localized photothermal heating following LSPR excitation plays an important role toward favoring the reaction step involving product desorption from the biocatalytic active sites, ultimately leading to increased reaction rates.

RESULTS AND DISCUSSION

The first step toward this study involves CALB adsorption onto Au NPs. It is well established that enzymes can interact with Au NP surfaces via the interaction of carboxyl and amine groups present in the amino acid residues of the enzyme structure, following a kinetic process that involves anchoring, crawling, and subsequent binding to the NP surface.[24,27,28] It has also been reported that electrostatic binding can take place between remaining carboxyl groups on the Au NP surface (e.g., from citrate employed during synthesis) and amino groups (e.g., Lys and Arg) from the enzyme structure.[29] Furthermore, enzymes containing thiolated amino acid residues may interact with the Au NP surface by chemisorption.[30,31] CALB presents 10 thiolated residues in its structure, of which four are methionine and six are cysteine residues, forming three disulfide bonds[32] and providing favorable conditions for anchoring enzymes onto the NP surface.[27]

AuNSt were synthesized using the seed-mediated growth method,[33,34] using ascorbic acid as a reducing agent, silver nitrate to assist the growth of spiky nanostructures, and CALB as a stabilizing molecule. AuNSp were synthesized according to the Turkevich method[35] and subsequently coated with CALB. Both AuNSt and AuNSp were washed by centrifugation and the supernatant was removed to ensure that only CALB molecules adsorbed onto the NP surface. AuNSt and AuNSp showed colloidal stability upon CALB adsorption. The corresponding nanobioconjugates are referred to as AuNSt@CALB and AuNSp@CALB, respectively. Figure 1A−D shows representative transmission electron microscopy (TEM) images of AuNSp@CALB (Figure 1A,B) and AuNSt@CALB (Figure 1C,D). The nanoparticle size distribution histograms are presented in Figure S1. The images confirm the formation of Au nanospheres and nanostars with a spiky morphology and sharp tips branching out from a central core. Both AuNSt@CALB and AuNSp@CALB displayed a relatively narrow size distribution, with diameters of 12 ± 2 and 100 ± 20 nm, respectively. For AuNSt, the tip dimensions were approximately 45 ± 5 nm in length and 5 ± 0.6 nm in width. Although not conclusive, the high-resolution TEM images (Figure 1B,D) evidenced the presence of an organic layer on AuNSp and AuNSt surfaces, which may correspond to adsorbed CALB. The morphologies of AuNSp and AuNSt were thus preserved upon CALB adsorption and no aggregation was observed, even after laser irradiation (Figure S2). This indicates that CALB served as a suitable stabilizing agent for both AuNSp and AuNSt. AuNSp@CALB and AuNSt@CALB exhibited intense LSPR bands around 525 nm and 700 nm, respectively (Figure 1E). These LSPR band positions were exploited to study the effect of on and off resonance conditions, relative to the NIR laser wavelength employed in CALB biocatalysis studies (808 nm, indicated by the dashed line shown in Figure 1E).

We then turned our attention to the study of CALB activity toward the hydrolysis of 4-nitrophenyl palmitate (*p*NPP) as a model reaction (see Scheme 1 in the Experimental section).

Scheme 1. Hydrolysis of *p*NPP Biocatalyzed by CALB[a]

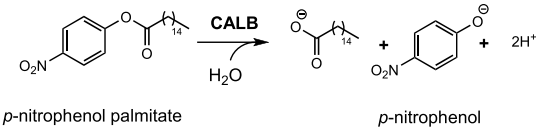

[a]The reaction rate can be monitored from *p*NP formation, by the absorbance at λ = 405 nm.

We found that CALB activity (under light-off conditions) decreased upon its adsorption on both AuNSt and AuNSp (Table 1). This behavior is a common trend typically observed for immobilized enzymes, being established that external mass transport restrictions limit their activity.[36] We determined the catalytic rate constant (k_{cat}), the binding Michaelis constant (K_M), and the catalytic efficiency (k_{cat}/K_M) of free CALB and the same apparent parameters for the adsorbed enzyme (Table 1 and Figure S3). Under light-off conditions, the decrease in k_{cat} values for CALB adsorbed on the Au NPs can be related to

https://dx.doi.org/10.1021/acscatal.0c04919
ACS Catal. 2021, 11, 414−423

Table 1. Kinetic Parameters Determined from Michaelis–Menten Plots (Figure S3) for Samples under Light on and off (Dark) Conditions[a]

	k_{cat} (min^{-1})		K_M (μM)		k_{cat}/K_M ($\mu M^{-1} \times min^{-1}$)	
sample	OFF	ON	OFF	ON	OFF	ON
AuNSt@CALB[b]	2461 ± 82	3947 ± 240	3.2 ± 0.4	5.1 ± 0.5	773 ± 180	765 ± 448
AuNSp@CALB[c]	2140 ± 126	2705 ± 372	4.8 ± 0.6	7.0 ± 2.0	443 ± 192	385 ± 186
free CALB[d]	15,855 ± 732	15,966 ± 758	10.4 ± 4.3	9.7 ± 3.9	1520 ± 169	1640 ± 192

[a]Reaction conditions: PBS buffer at pH 7.4; at room temperature (~20 °C); NIR laser irradiation at 3.2 W/cm^2. Enzyme concentration used: [b]1.5 μmol L^{-1}, [c]1.0 μmol L^{-1}, [d]1.1 μmol L^{-1}. The kinetic constants calculated for the immobilized enzymes are apparent constants since they also account for mass transfer restrictions.

a partial loss of enzyme activity. Nevertheless, the K_M values for the adsorbed enzyme on the Au NPs were significantly smaller as compared to free CALB. This lower apparent K_M suggests an increase of the substrate local concentration at the NP surface, which causes the higher activities observed at a lower bulk substrate concentration. This effect was more evident for AuNSt than for AuNSp. Similar results were obtained with a homologous lipase from *Candida rugosa* immobilized on AuNSp.[26] The k_{cat}/K_M values decreased upon CALB adsorption on the Au NPs, but that decay was 1.7 times lower for AuNSt@CALB than for AuNSp@CALB. The different kinetic behaviors of CALB on the two different NP morphologies can be related to the enzyme density found in nanoparticles with different curvatures, where NPs with a smaller size (i.e., with a higher curvature) display a higher enzyme activity.[23] In this context, the tips of AuNSt (ca. 5 nm in diameter) can provide a surface of a much higher curvature, compared to AuNSp (diameter around 12 nm), leading to a lower density of CALB at the NP surface, which results in a higher enzyme activity.

We further studied the effect of light irradiation on the hydrolytic activity of AuNSt@CALB and AuNSp@CALB under different irradiation conditions. The reactions were carried out in a quartz cuvette illuminated with an NIR laser at λ = 808 nm, measuring the release of 4-nitrophenolate (*p*NP) in situ, using a UV–vis spectrophotometer (Figure 2A). Unlike the results under dark conditions, NIR irradiation enhanced the enzymatic activity of AuNSt@CALB to a significantly higher extent than that for AuNSp@CALB irradiated under different laser powers (Figure 2B and Table 1). This result agrees with the better match between the incoming light wavelength (808 nm) and the LSPR position in AuNSt (700 nm, Figure 1E), as compared to AuNSp (525 nm, Figure 1E). In the case of AuNSt@CALB, the activity increased with the laser power until reaching a plateau at laser powers above 1.6 W/cm^2. No differences were observed for the activity of free CALB under light on and off conditions (Figure S4). Therefore, NIR irradiation only leads to a significant enhancement of the activity of CALB molecules at the surface of AuNSt, which feature an LSPR position that better matches the light excitation wavelength.

To unravel the effect of LSPR excitation on the enzymatic activity, we investigated the heating capacity of AuNSt and AuNSp under the employed light irradiation conditions. The samples were therefore illuminated with the NIR laser, and the temperature changes in the colloidal dispersion over time were monitored with a thermal camera. When the temperature reached thermal equilibrium, the laser was turned off and the cooling down curve was recorded to quantify heat dissipation to the solution. Figure 3A shows exemplary heating and cooling curves for both AuNSt@CALB and AuNSp@CALB. The molar heat transfer rates for both AuNSt and AuNSp were calculated by fitting these temperature-time courses to eq 1,[37] as illustrated in Figure 3B.

$$\frac{\Delta Q}{c_{Au}} = \frac{Q_{sample} - Q_{medium}}{\varepsilon_{400}/2.4\ mmol\ L^{-1}} \quad (1)$$

Here, the generated heat output (ΔQ), obtained from the heat difference between the sample (Q_{sample}) and the medium (Q_{medium}), is related in terms of the gold concentration ($c_{Au} = \varepsilon_{400}/2.4$ mmol L^{-1})[38] in the sample. It was found that the molar heat transfer rate was much larger for AuNSt@CALB than for AuNSp@CALB. In this case, the LSPR excitation leads to photothermal heating because of plasmon decay. Such a photothermal heating effect takes place close to the NP surface and is further dissipated to the reaction mixture, leading to the detected temperature increase. Our data indicate that AuNSt are more efficient nanosources of heat[8] than AuNSp under the employed NIR irradiation conditions. In

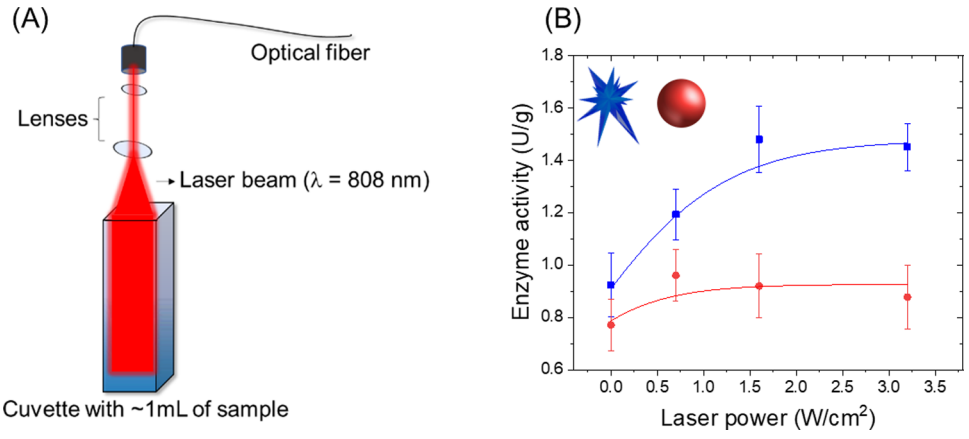

Figure 2. (A) Schematic illustration of the laser irradiation setup. (B) Effect of NIR laser power (λ = 808 nm) on the enzymatic activity of AuNSt@CALB (blue squares) and AuNSp@CALB (red circles).

https://dx.doi.org/10.1021/acscatal.0c04919
ACS Catal. 2021, 11, 414–423

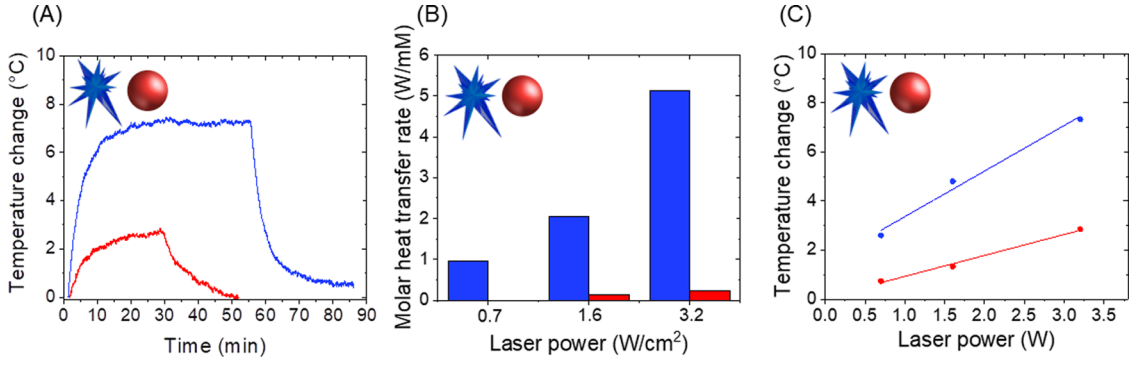

Figure 3. Plasmonic heating effects of NIR laser (λ = 808 nm) on AuNSt@CALB (blue) and AuNSp@CALB (red). (A) Example of heating and cooling curves (laser power 3.2 W/cm^2). (B) Molar heat transfer rate vs laser power. (C) Temperature changes measured in colloidal dispersions of AuNSt@CALB (blue) and AuNSp@CALB (red).

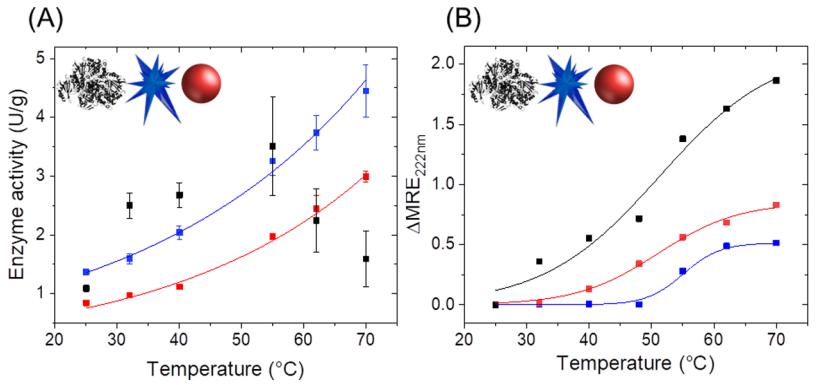

Figure 4. Temperature effects under dark conditions on the enzymatic activity (A) and the enzyme secondary structure (B) for AuNSt@CALB (blue), AuNSp@CALB (red), and free CALB (black). (A) Enzymatic activity as a function of temperature, fitted to the Arrhenius model. (B) Thermal denaturation of the enzyme conformation monitored by the variation of MRE (ΔMRE = MRE$_{25°C}$ − MRE$_T$) at 222 nm, measured by CD spectroscopy. CD data were obtained from an average of 10 accumulation spectra for each sample.

fact, Figure 3C shows that AuNSt@CALB under NIR irradiation (3.2 W/cm^2) were capable of increasing the bulk temperature of the reaction mixture up to 7.3 °C, versus the 2.7 °C observed for AuNSp@CALB under the same conditions. As expected from the photothermal heating triggered by LSPR excitation, we observed an increase in the bulk temperature on increasing the laser power.

In this context, it is expected that photothermal heating can lower the activation energy of the enzyme, according to the Arrhenius analysis,[22] thereby leading to a higher enzyme activity. This effect was further confirmed by activity assays for both free CALB and enzymes adsorbed onto Au NPs at different temperatures, as shown in Figure 4A. Typically, each class of enzyme exhibits an optimal temperature at which the highest activity is observed.[39] Above this value, the activity gradually decreases due to protein denaturation. Free CALB showed an optimal temperature of 55 °C (Figure 4A), in agreement with previously reported data.[40] At temperatures above 55 °C, free CALB undergoes thermal deactivation and its activity decreases considerably. Conversely, the enzymatic activity increased with temperature, even at values above 55 °C, for AuNSt@CALB and AuNSp@CALB. The preservation of the enzyme activity at high temperatures indicates that the adsorption of CALB on Au NPs enhances the enzyme thermal stability. Circular dichroism (CD) spectroscopy studies (Figure 4B and Figure S5) demonstrate the higher conformational stability of enzymes adsorbed on both AuNSt and AuNSp, which explains their higher enzyme activities at temperatures above 55 °C. The observed decrease in mean residue ellipticity (MRE) at 222 nm corresponds to major conformational changes in the α-helix secondary structure of CALB (Figure 4B). The adsorption of CALB on AuNSt precludes the structural distortions induced by the higher temperatures, as no significant ellipticity changes were observed up to 48 °C. However, the conformation of free CALB was gradually distorted at temperatures higher than 25 °C.

Interestingly, the activity vs temperature correlation (Figure 4A) serves as a calibration curve for the indirect evaluation of local gradients occurring under irradiation conditions (Figure 2B). This strategy has been previously used to determine the local heating of magnetic iron oxide nanoparticles under alternating magnetic fields.[41] As presented in Figure 2B, the enzymatic activity of AuNSt@CALB under 3.2 W/cm^2 laser irradiation was 58% higher than that under nonirradiated conditions at the same bulk temperature (room temperature). We know that the particles under 3.2 W/cm^2 laser irradiation were only capable of heating the bulk up to 32 °C (Figure 3C). However, a proportional activity enhancement of 58% would correspond to a bulk temperature of roughly 42 °C (see Figure 4A). The differences between the expected activity according to the bulk temperature correlation (Figure 4A) and the measured activity under laser irradiation (Figure 2B) suggest the existence of a local temperature gradient between the AuNSt surface and the bulk. In this way, based on the obtained enzyme activity values, we estimated a 10 °C gradient

https://dx.doi.org/10.1021/acscatal.0c04919
ACS Catal. 2021, 11, 414−423

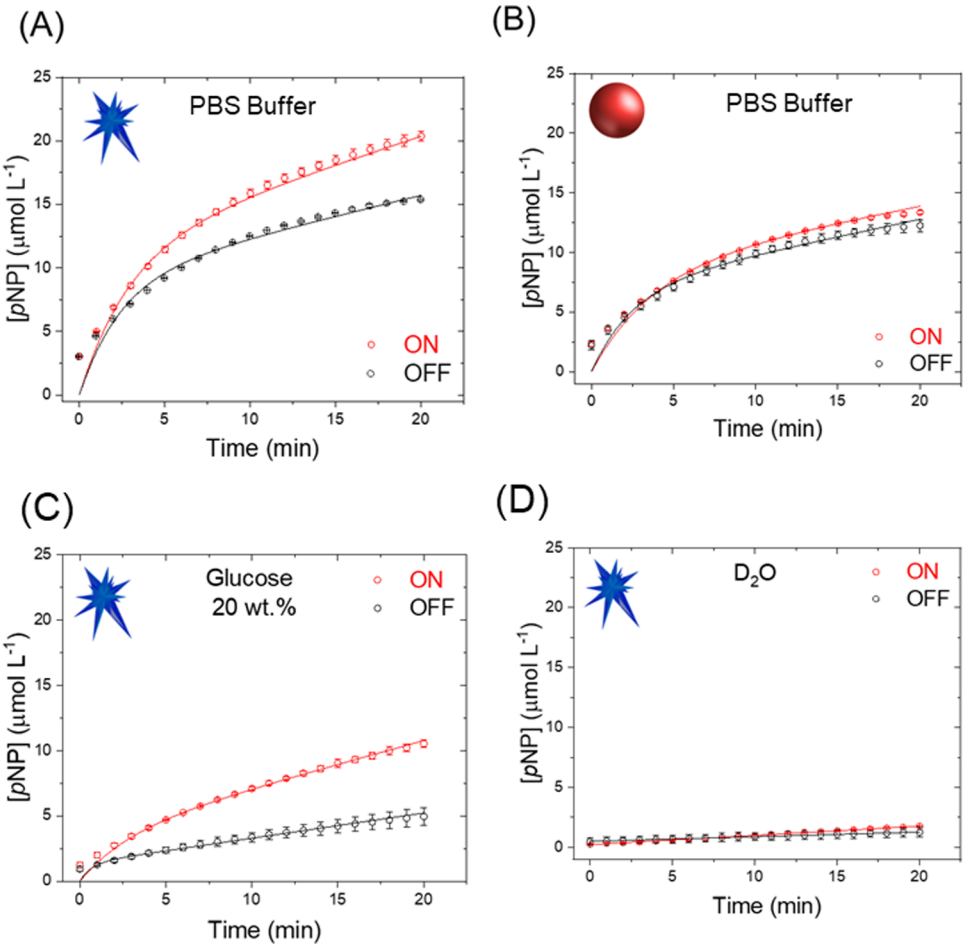

Figure 5. Time courses of *p*NPP hydrolysis catalyzed in PBS buffer (A and B) by AuNSt@CALB (A, C, and D) and AuNSp@CALB (B), under NIR irradiation (3.2 W/cm^2) and nonirradiation (dark) conditions. Viscosity (C) and solvent isotopic (D) effects on the time dependence of the product formation for AuNSt@CALB. Viscosity assays were performed in the presence of glucose 20 wt %, and solvent isotopic assays were performed in the presence of D_2O. All experimental data were fitted to an initial-burst kinetic model (eq 2) and the respective values are listed in Table S1.

difference between the enzyme environment (42 °C) and the bulk (32 °C). This observation may also be related to previous studies describing the inactivation of enzymes immobilized on Au NPs under laser irradiation, likely due to excess local heating.[10,11]

Previous studies have described similar observations on the thermal effects promoted by light absorption.[10−15] Recently, the effects of photothermal heating and LSPR-excited charge carriers were investigated in plasmonic catalysis,[4,8,9] but a clear distinction of their contributions remains challenging. This is because photothermal heating is largely unavoidable following LSPR excitation.[42] In the present case, AuNSt seem to release more photothermal heat to the surrounding media as a result of more efficient LSPR excitation,[8,43] leading to a larger enhancement in the enzyme activity. Moreover, it is plausible that water pocket interfaces present in the enzyme structure can result in higher yields of energy distribution throughout the enzyme structure.[44] Lastly, we argue that discussing the activity enhancement mechanism through a mechanism based on LSPR-excited charge carriers would be too speculative as the hydrolysis mechanism does not involve electron transfer and CALB lacks any metallic center that may facilitate electron shuttle. Although both mechanisms might occur simultaneously, electronic effects can be hardly assessed for this system using state-of-the-art methodologies, whereas photothermal effects are more accessible as we showed.

Inspired by these results, we performed a series of studies to understand the effect of LSPR excitation on the activity enhancement observed for AuNSt@CALB through the determination of the steady-state kinetic parameters under irradiation conditions. First of all, we investigated how the maximum reaction rate and k_{cat} were affected by light irradiation when CALB was adsorbed on Au NPs (Table 1 and Figure S3). The value of the apparent k_{cat} is 60% higher for AuNSt@CALB under irradiation than under nonirradiation conditions. This effect was less noticeable for AuNSp@CALB and even less for free CALB. Interestingly, K_M values increased under laser irradiation only when CALB was adsorbed on Au NPs, with no apparent changes in free CALB, suggesting that laser irradiation influences the enzymatic activity when CALB is at the Au NP surface. The k_{cat}/K_M showed similar values for all samples, regardless of light irradiation, because the effect of light on the catalytic constant is compensated by the effect on the binding constant. The higher k_{cat} values under irradiation conditions are probably due to the higher local temperature at the surface of AuNSt, which is also supported by the analysis based on Arrhenius plots (Figure S6). The activation energy barrier for the enzyme activity on AuNSt@CALB decreased

https://dx.doi.org/10.1021/acscatal.0c04919
ACS Catal. 2021, 11, 414−423

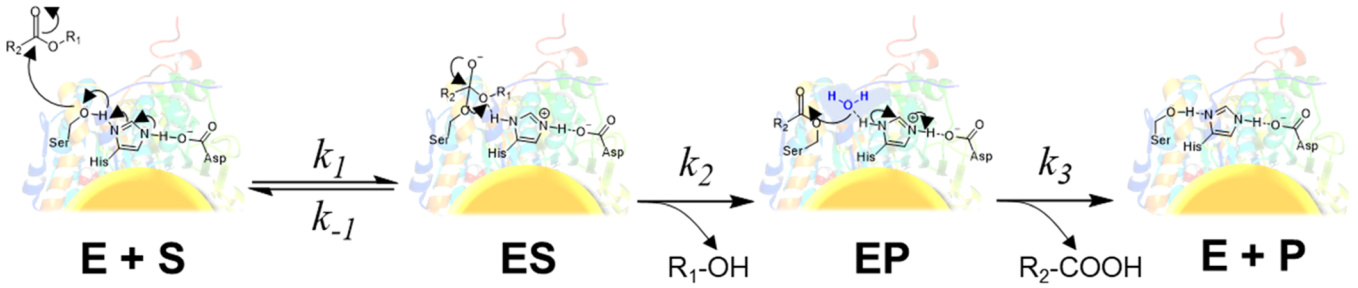

Figure 6. Scheme of the general mechanism for a lipase catalytic reaction. The constants k_1 and k_{-1} are related to reversible binding of the substrate (S) to the enzyme (E) active site, to form the transient intermediate (ES); k_2 rules the formation of the acyl−enzyme complex and release of the alcohol product (EP); k_3 accounts for the hydrolysis of that complex, releasing the acid product to the bulk (E + P).

from 32 to 21 kJ mol^{-1} when the laser was turned on. In contrast, light was unable to alter the activation energy of the free enzyme, supporting that the interface between the enzyme and AuNSt played a key role in enhancing the enzymatic activity through plasmonic effects.

We next performed a more detailed analysis of the reaction time courses that revealed fundamental mechanistic information on the performance of CALB adsorbed on Au NPs, under light irradiation conditions (Figure 5). According to the general enzymatic mechanism (see Figure 6), the reaction kinetics are driven by an initial fast equilibrium binding step followed by an irreversible chemical step. Assuming that the second step of the lipase reaction is the rate-limiting one, the activity assay we used does not account for the product release of the acid,[28,45,46] since the colorimetric method only detects the product *p*NP. The reaction time courses shown in Figure 5 were fitted to the initial-burst kinetic model as described by eq 2, to better estimate the second step of the lipase mechanism.[47]

$$[P] = vt + [E_0] \times (1 - e^{-k_{obs}t}) \quad (2)$$

Here, the concentration of the formed product (P) is related to the initial velocity (v), the initial concentration of the enzyme (E_0), and the rate constant (k_{obs}) as a function of time (t) (see Figure S7). In this kinetic model, if $k_{obs} \gg v$, v accounts for the rate-limiting step in the enzymatic mechanism of CALB, which we assign to the steps of hydrolysis of the acyl−enzyme complex and product release. Looking beyond the initial burst in the early stages of product conversion with AuNSt@CALB, Figure 5A illustrates that light irradiation affects more significantly the second phase (after ca. 5 min) of the time courses. Indeed, AuNSt@CALB exhibited a v value which is 36% higher under irradiation than under nonirradiation (dark) conditions. Such a light-driven enhancement was higher than that observed for AuNSp@CALB (12%) (Figure 5B). The time course conversion as a function of time for free CALB did not fit this kinetic model, but the Michaelis−Menten kinetic parameters clearly demonstrate that the activity of the free enzyme was not affected by light irradiation. Consequently, laser irradiation appears to play a relevant role in the rate-limiting step of the enzyme reaction mechanism.

To explain the effect of light on the CALB activity from a mechanistic point of view, we inspected the well-known three-step catalytic mechanism of hydrolases (Figure 6).[23,26,45,48,49] This mechanism is defined by four distinct rate constants (k_1, k_{-1}, k_2, and k_3).[26,45,49] Therefore, to decipher whether light affects either the chemical hydrolysis, or the product release or both steps, reaction-time courses were recorded with AuNSt@CALB in different reaction media, under both light and dark conditions.

We first monitored reaction-time courses in viscous media (20 wt % glucose), aiming at hampering the product diffusion out of the active center (state E + P). The interchain hydrogen bonds formed between glucose molecules increase the medium viscosity,[50] like other sugar solutions such as sucrose,[22,23] which is known to hamper the product release from the enzyme microenvironment. Under these conditions, the product release appears to be the dominant rate-limiting step,[23,48] so the effects of laser irradiation on the v parameter of the initial-burst model compared to the corresponding control experiments (no glucose) can be quantified. Under both on and off conditions, the more viscous reaction media slowed down product formation along time (Figure 5C and Table S1). Remarkably, light irradiation significantly accelerated (by 40%) the slowest phase of the time courses using AuNSt@CALB under viscous conditions. Conversely, the influence of light on the performance of both AuNSp@CALB and free CALB was negligible (Figure S8). To confirm the results extracted from the burst kinetic model, and considering the deacylation of the enzyme as the slower step (i.e., $k_3 \ll k_2$), which means that k_3 is the rate-limiting step (i.e., $k_{cat} = k_3$) as supported by recent computational studies,[51] we constructed the three-step kinetic model shown in Figure 6 using the software COPASI.[52] This model allowed us to estimate k_3 values from the reaction courses obtained with AuNSt@CALB (see Table S2 and Figure S9). We found that k_3 follows the same trend as the v parameter calculated from the initial-burst kinetic model. Light increases the k_3 value of AuNSt@CALB by twofold, compared to the nonirradiated reaction, and the $k_{3(ON)}/k_{3(OFF)}$ ratio is maximized under viscous reaction media (in the presence of glucose) by a factor of 3.5 (Figure S10). These experimental results suggest that light contributes to enhancing the catalytic properties of AuNSt@CALB through easing the product release (state E + P) from the enzyme close to the plasmonic NP surface. Subsequently, to evaluate whether light can also affect the kinetics of the hydrolytic step (state EP), the kinetic isotopic effect (KIE)[53] was studied using heavy water (D_2O) under laser on and off conditions, and the results were compared to their corresponding control experiments (in H_2O). In this step, water molecules from the medium played a crucial role in the nucleophilic attack for cleaving the carbonyl group bond of the acyl−enzyme complex.[26,49] When using D_2O as the solvent, the enzyme activity dramatically decreased for both conditions, as expected from the occurrence of an isotopic effect in the hydrolysis step[53] (Figure 5D). Hence, we observe a KIE of $v(H_2O)/v(D_2O)$ of 8.67, which demonstrates that the hydrolysis of the acyl−enzyme complex dominates the

https://dx.doi.org/10.1021/acscatal.0c04919
ACS Catal. 2021, 11, 414−423

rate-limiting step (k_3). On the other hand, when the reaction-time courses were recorded in the presence of D_2O and under irradiation conditions, light had a negligible effect on the enzymatic rates. Hence, when the hydrolysis of the acyl−enzyme complex is extremely slow due to isotopic effects, NIR laser irradiation no longer affects the rate-limiting step of the AuNSt@CALB catalysis mechanism. Interestingly, these results indicate that plasmonic excitation hardly affects the kinetics of water attack, while it significantly increases the efficiency of the product-release step. When compared to the activity of soluble CALB measured in a PBS buffer, we found a stronger temperature dependence of the free enzyme activity in viscous media but a weaker dependence in D_2O. These results further support the enhancement of the product release when the enzyme is locally heated at the interface with the irradiated plasmonic nanoparticles (Figure S11). Previous studies, which reported that enzyme immobilization on the surface of nanoparticles leads to more significant changes in the product-release step in the enzymatic kinetics,[22,23] also support the assumption that the major contribution of light is related to this step. Therefore, our results demonstrate that LSPR excitation increases the activity of AuNSt@CALB by enhancing the kinetics of product release in the last step of the enzyme mechanism driven by k_3, as summarized in Figure 6. This effect has been observed exclusively with AuNSt@CALB, confirming that the LSPR of Au NPs must be in resonance with the incident NIR laser wavelength (808 nm), to exert the effect on enzyme properties.

CONCLUSIONS

We used CALB adsorbed on the surface of AuNSp and AuNSt as a model system to unravel the effect of light illumination, and thus LSPR excitation, on the underlying mechanisms behind the plasmonic enhancement of enzyme activity under NIR excitation. It was found that LSPR excitation in the NIR enabled an increase of 58% in the enzyme activity when AuNSt were employed as immobilization carriers. In addition to the enhanced activities, we investigated the effect of plasmonic excitation on the rate-limiting step of the enzymatic reaction. Data from highly viscous conditions and solvent isotopic effects revealed that photothermal heating from LSPR excitation accelerated the last step of the reaction by favoring product release, rather than improving the hydrolytic step at the interface between the enzyme and the plasmonic NPs. We envision that some of the mechanistic conclusions reached in this work can be translated to other combinations of enzymes and plasmonic NPs and may inspire the rational design of plasmonic NPs and enzyme hybrids with target activities and selectivity that can be externally controlled by light excitation.

EXPERIMENTAL SECTION

Materials. Lipase from *Candida antarctica* fraction B (CALB), tetrachloroauric acid ($HAuCl_4.3H_2O$), sodium citrate tribasic dihydrate, ascorbic acid, silver nitrate, and 4-nitrophenyl palmitate were purchased from Sigma-Aldrich. Phosphate-buffered saline was purchased from Biochrom GmbH (Berlin, Germany). CALB solutions were prepared in PBS buffer of pH 7.4. The concentration of CALB was determined using the Bradford colorimetric assay kit,[54] purchased from Thermo Scientific. All chemicals were used as received. Purified Milli-Q water (Millipore, 18.2 MΩ cm) was used in the preparation of all solutions.

Gold Nanoparticle Synthesis and CALB Adsorption. *AuNSp@CALB Synthesis.* AuNSp were obtained using the Turkevich method.[55] In a typical procedure, 150 mL of 2.2 mmol L^{-1} of sodium citrate solution under vigorous stirring was heated until boiling. Then, 1 mL of 25 mmol L^{-1} of $HAuCl_4$ was added. The temperature was decreased to ∼90 °C and the solution color changed from soft yellow to red in ∼10 min. After the solution reached 90 °C, 1 mL of 60 mmol L^{-1} of sodium citrate solution and 1 mL of 25 mmol L^{-1} of $HAuCl_4$ were subsequently added and stirred for 30 min at 90 °C. After cooling to room temperature, the samples were stored in a fridge for further use. The adsorption of CALB onto AuNSp to obtain AuNSp@CALB bioconjugates was adopted from a previously described method.[24] First, 0.1 mg mL^{-1} of CALB stock solutions were prepared in a PBS buffer of pH 7.4. A volume of 10 mL of CALB solution was added to 10 mL of previously synthesized AuNSp. The sample was incubated for 2 h at 32 °C and 300 rpm in an Eppendorf thermomixer. Before use, the colloidal dispersion was washed by centrifugation at 13,000 rpm for 20 min to remove excess CALB and possible nonreactants during AuNSp synthesis. The precipitate was washed and redispersed in PBS buffer. Samples were previous analyzed by UV−vis spectroscopy (Agilent 8453) to monitor the LSPR and to determine the molar gold concentration in the samples at λ = 400 nm.[38] The final concentration of Au in AuNSp@CALB was 0.84 μmol L^{-1} and that of CALB was 1.06 μmol L^{-1}.

AuNSt@CALB Synthesis. AuNSt@CALB synthesis was adopted from a previously described method.[33,34] AuNSt were obtained by seed-mediated growth. First, a seed solution was prepared by adding 5 mL of 34 mmol L^{-1} of sodium citrate into 95 mL of 0.5 mmol L^{-1} of $HAuCl_4$ under boiling and vigorous stirring, and stirring was continued for 15 min at the same temperature. After cooling to room temperature, the colloidal dispersion was stored in a fridge for further use. For AuNSt synthesis, 100 μL of 25 mmol L^{-1} of $HAuCl_4$ was added into 10 mL of H_2O containing 10 μL of 1 mmol L^{-1} of HCl under vigorous stirring at room temperature. Then, 100 μL of seed solution, 100 μL of 3 mmol L^{-1} of silver nitrate solution, and 50 μL of 100 mmol L^{-1} of ascorbic acid solution were quickly added subsequently. After 3−5 min of stirring, 10 mL of 0.1 mg mL^{-1} of CALB solution was added and stirred for 5 min. Then, the sample was stored in a fridge for further use. Samples were washed just before use by centrifugation at 7000 rpm for 15 min to remove excess CALB and possible nonreactants during AuNSt synthesis. The precipitate was washed and redispersed in PBS buffer. Samples were previous analyzed by UV−vis spectroscopy (Agilent 8453) to monitor the LSPR signal and to determine the molar gold concentration in the samples at λ = 400 nm.[38] The final concentration of Au in AuNSt@CALB was 0.54 μmol L^{-1} and that of CALB was 1.14 μmol L^{-1}.

Enzymatic Activity Assays. *pNPP Hydrolysis Time Dependence of the Product Formation.* The enzymatic activities of free CALB and CALB−AuNSp bioconjugates were determined by measuring the release of *p*NP from the hydrolysis of *p*NPP (Scheme 1), monitored by UV−vis spectroscopy at λ = 405 nm, as previously described elsewhere.[24,26] In a quartz cuvette containing 1000 μL of PBS buffer at pH 7.4, 36 μL of 0.5 mmol L^{-1} of *p*NPP solution previously prepared in isopropanol was added. All *p*NPP solutions were prepared on the same day. Subsequently, 36 μL of the sample was added and homogenized. The solution color

https://dx.doi.org/10.1021/acscatal.0c04919
ACS Catal. 2021, 11, 414−423

changed slowly from transparent to light yellow upon *p*NP release, corresponding to the amount of CALB in the sample. The *p*NP concentration was determined from Lambert−Beer's law using a molar extinction coefficient of ε = 12,800 mol L^{-1} cm^{-1}.[26] The enzymatic activity was determined from the initial velocity obtained from the linear slope of *p*NP concentration versus time plot. The unit U/g corresponds to 1 μmol of the product *p*NP formed per 1 min of reaction corresponding to the amount of protein. For the assays upon laser illumination, the cuvette was illuminated vertically (see the scheme shown in Figure 2A). Absorbance related to *p*NP formation were recorded at each 1 min for approximately 20 min.

Michaelis−Menten Model. The enzymatic kinetics of free CALB and CALB−AuNP bioconjugates were determined using the typical procedure of the Michaelis−Menten model.[28,56] First, *p*NPP solutions at initial concentrations of 0.5, 0.4, 0.3, 0.2, 0.1, 0.05, and 0.01 mmol L^{-1} were prepared in isopropanol. All *p*NPP solutions were prepared on the same day before use. The same procedure described in the previous section for *p*NPP hydrolysis time dependence of the product formation to determine the enzyme activity was performed. The values of the parameters, maximum velocity (V_{max}) and Michaelis−Menten constant (K_M), related to the initial velocity (V_o) and substrate concentration ($[S]$), were obtained from the typical relation

$$V_o = \frac{V_{max} \times [S]}{K_M + [S]} \tag{3}$$

Arrhenius Analysis. Arrhenius analysis was performed to determine the enzyme activation energy of free CALB and CALB−AuNP bioconjugates as described previously elsewhere.[22] The enzyme activity was determined using the same procedure described in the former section for *p*NPP hydrolysis, by varying the temperature from 25 to 80 °C. The values of activation energy (E_a) were obtained from a linear fitting using the relation described below

$$\ln K = \ln A - \frac{E_a}{RT} \tag{4}$$

where, K is the rate constant, A is the preexponential factor, and R is the universal gas constant at the absolute temperature (T).

Viscosity and Solvent Isotope Dependence. Viscosity and solvent isotope dependence kinetics were performed as previously described elsewhere.[23,48] For the viscosity assays, kinetics were performed in the presence of 20 wt % glucose prepared in PBS buffer. For the solvent isotope assays, kinetics were performed in the presence of D_2O. All samples were previously washed and resuspended in D_2O to avoid any water molecules during the kinetic measurements. The enzyme activity was determined using the same procedure described in the previous section for *p*NPP hydrolysis time dependence of the product formation. Data were analyzed and fitted using an initial burst of the product kinetics model.[47]

Heating Experiments. A volume of 1 mL of sample in a quartz cuvette was illuminated using an NIR laser at λ = 808 nm (fiber-coupled laser diode, Lumics LU0808T040) laterally, passing through two lenses, one to collimate and the other to expand the laser beam in order to illuminate a spot of 1 cm^2 on the sample. The laser was illuminated for different powers (0.7, 1.6, and 3.2 W/cm^2) and monitored using a thermal camera (FLIR A35) placed above the cuvette. The heating and cooling curves were obtained from the thermal camera data using ResearchIR software. PBS buffer and water were selected as blank curves to eliminate any contribution from the medium. The molar heat rate transfer was calculated using eq 1.[37]

Characterization Techniques. *Transmission Electron Microscopy.* TEM images were obtained using a JEOL microscope at an acceleration voltage of 200 kV. Approximately 3 μL of sample was dropped on a lacey carbon-coated grid and left to dry. The size distribution of the nanoparticles obtained was analyzed using ImageJ software.

Circular Dichroism Spectroscopy. CD measurements were obtained using a Jasco J-815 CD spectrometer. CD spectra were recorded in the range of 200−260 nm, using a quartz cuvette of 5 mm, bandwidth of 5 nm, data pitch of 1 nm, and scanning speed of 50 nm/min. The spectra were obtained from an average of 10 accumulations and corrected by the PBS buffer spectrum. The measurements were expressed in terms of MRE using the relation

$$\mathrm{MRE} = \frac{\mathrm{MRW} \times \theta}{10dC} \tag{5}$$

where, the measured ellipticity (θ) in degrees is related to the cuvette path length (d) in centimeters and the protein concentration (C) in g mL^{-1}. MRW corresponds to the mean residue weight defined by MRW = $M/(N-1)$, where M is the molecular mass in Daltons and N is the number of amino acids in the protein structure. For CALB, M = 33,000 g mol^{-1} and N = 317.[40]

■ ASSOCIATED CONTENT

Supporting Information

The Supporting Information is available free of charge at https://pubs.acs.org/doi/10.1021/acscatal.0c04919.

Additional information on LSPR characterization before and after NIR laser irradiation; Michaelis−Menten plots; NIR laser power effect on free CALB; CD spectra as a function of temperature; Arrhenius plots, example of initial burst of product kinetics; viscosity on time dependence of the product formation; fitting data carried out with COPASI and the values obtained; table containing parameters obtained from the fitted kinetics data and from COPASI software (PDF)

■ AUTHOR INFORMATION

Corresponding Authors

Heloise Ribeiro de Barros − *Department of Fundamental Chemistry, Institute of Chemistry, University of São Paulo, 05508-000 São Paulo, Brazil; CIC biomaGUNE, Basque Research and Technology Alliance (BRTA), 20014 Donostia − San Sebastián, Spain;* orcid.org/0000-0003-2700-7803; Email: barroshr@usp.br

Fernando López-Gallego − *CIC biomaGUNE, Basque Research and Technology Alliance (BRTA), 20014 Donostia − San Sebastián, Spain; Ikerbasque, Basque Foundation for Science, 48013 Bilbao, Spain;* orcid.org/0000-0003-0031-1880; Email: flopez@cicbiomagune.es

Authors

Isabel García − *CIC biomaGUNE, Basque Research and Technology Alliance (BRTA), 20014 Donostia − San Sebastián, Spain; Centro de Investigación Biomédica en Red,*

https://dx.doi.org/10.1021/acscatal.0c04919
ACS Catal. 2021, 11, 414−423

Bioingeniería, Biomateriales y Nanomedicina (CIBER-BBN), 20014 Donostia – San Sebastián, Spain

Christian Kuttner – *CIC biomaGUNE, Basque Research and Technology Alliance (BRTA), 20014 Donostia – San Sebastián, Spain*

Nicoll Zeballos – *CIC biomaGUNE, Basque Research and Technology Alliance (BRTA), 20014 Donostia – San Sebastián, Spain*

Pedro H. C. Camargo – *Department of Fundamental Chemistry, Institute of Chemistry, University of São Paulo, 05508-000 São Paulo, Brazil; Department of Chemistry, University of Helsinki, Helsinki 00100, Finland;* orcid.org/0000-0002-7815-7919

Susana Inés Cordoba de Torresi – *Department of Fundamental Chemistry, Institute of Chemistry, University of São Paulo, 05508-000 São Paulo, Brazil;* orcid.org/0000-0003-3290-172X

Luis M. Liz-Marzán – *CIC biomaGUNE, Basque Research and Technology Alliance (BRTA), 20014 Donostia – San Sebastián, Spain; Centro de Investigación Biomédica en Red, Bioingeniería, Biomateriales y Nanomedicina (CIBER-BBN), 20014 Donostia – San Sebastián, Spain; Ikerbasque, Basque Foundation for Science, 48013 Bilbao, Spain;* orcid.org/0000-0002-6647-1353

Complete contact information is available at: https://pubs.acs.org/10.1021/acscatal.0c04919

Author Contributions

The manuscript was written through contributions of all authors. All authors have given approval to the final version of the manuscript.

Notes

The authors declare no competing financial interest.

■ ACKNOWLEDGMENTS

The authors thank Brazilian agencies CNPq and São Paulo Research Foundation FAPESP (2015/26308-7 and 2018/13492-2) for financial support. H.R.B. also thanks FAPESP for the fellowships granted (2019/09668-0 and 2017/20892-4). P.H.C.C. thanks FAPESP, the University of Helsinki, and the Jane and Aatos Erkko Foundation for support. C.K. acknowledges funding from the European Union's Horizon 2020 research and innovation program under the Marie Skłodowska-Curie grant agreement No. 799393 (NANOBIOME). L.M.L-.M. and I.G. acknowledge funding from the Spanish State Research Agency (Grant MAT2017-86659-R). Funding from IKERBASQUE to L.M.L-.M. and F.L-.G. is also acknowledged. This work was performed under the Maria de Maeztu Units of Excellence Program from the Spanish State Research Agency—Grant No. MDM-2017-0720.

■ ABBREVIATIONS

Au NPs,gold nanoparticles; AuNSp,gold nanospheres; AuNSt,-gold nanostars; CALB,*Candida antarctica* fraction B; CD,circular dichroism; k,rate constant; k_{cat},apparent catalytic rate; k_{cat}/K_M,catalytic efficiency; KIE,kinetic isotopic effect; K_M,Michaelis constant; LSPR,localized surface plasmon resonance; MRE,mean residue ellipticity; NIR,near-infrared; *p*NP,4-nitrophenolate; *p*NPP,4-nitrophenyl palmitate; TEM,-transmission electron microscopy.

■ REFERENCES

(1) Mosquera, J.; Zhao, Y.; Jang, H. J.; Xie, N. L.; Xu, C. L.; Kotov, N. A.; Liz-Marzán, L. M. Plasmonic Nanoparticles with Supramolecular Recognition. *Adv. Funct. Mater.* **2019**, *30*, 1−17.

(2) Litti, L.; Reguera, J.; de Abajo, F. J. G.; Meneghetti, M.; Liz-Marzán, L. M. Manipulating Chemistry Through Nanoparticle Morphology. *Nanoscale Horiz.* **2020**, *5*, 102−108.

(3) Bodelón, G.; Costas, C.; Pérez-Juste, J.; Pastoriza-Santos, I.; Liz-Marzán, L. M. Gold Nanoparticles for Regulation of Cell Function and Behavior. *Nano Today* **2017**, *13*, 40−60.

(4) Liz-Marzán, L. M.; Murphy, C. J.; Wang, J. F. Nanoplasmonics. *Chem. Soc. Rev.* **2014**, *43*, 3820−3822.

(5) Araujo, T. P.; Quiroz, J.; Barbosa, E. C. M.; Camargo, P. H. C. Understanding Plasmonic Catalysis with Controlled Nanomaterials Based on Catalytic and Plasmonic Metals. *Curr. Opin. Colloid Interface Sci.* **2019**, *39*, 110−122.

(6) Linic, S.; Aslam, U.; Boerigter, C.; Morabito, M. Photochemical Transformations on Plasmonic Metal Nanoparticles. *Nat. Mat.* **2015**, *14*, 567−576.

(7) Wang, H.; Liu, T.; Huang, Y. Z.; Fang, Y. R.; Liu, R. C.; Wang, S. X.; Wen, W. J.; Sun, M. T. Plasmon-Driven Surface Catalysis in Hybridized Plasmonic Gap Modes. *Sci. Rep.* **2014**, *4*, No. 07087.

(8) Baffou, G.; Quidant, R. Thermo-Plasmonics: Using Metallic Nanostructures as Nano-Sources of Heat. *Laser & Photonics Rev.* **2013**, *7*, 171−187.

(9) Baffou, G.; Quidant, R. Nanoplasmonics for Chemistry. *Chem. Soc. Rev.* **2014**, *43*, 3898−3907.

(10) Guo, S. J.; Li, H.; Liu, J.; Yang, Y. M.; Kong, W. Q.; Qiao, S.; Huang, H.; Liu, Y.; Kang, Z. H. Visible-Light-Induced Effects of Au Nanoparticle on Laccase Catalytic Activity. *ACS Appl. Mater. Interfaces* **2015**, *7*, 20937−20944.

(11) Bretschneider, J. C.; Reismann, M.; von Plessen, G.; Simon, U. Photothermal Control of the Activity of HRP-Functionalized Gold Nanoparticles. *Small* **2009**, *5*, 2549−2553.

(12) Blankschien, M. D.; Pretzer, L. A.; Huschka, R.; Halas, N. J.; González, R.; Wong, M. S. Light-Triggered Biocatalysis Using Thermophilic Enzyme-Gold Nanoparticle Complexes. *ACS Nano* **2012**, *7*, 654−663.

(13) Li, W.; Liu, D. N.; Geng, X.; Li, Z. Q.; Gao, R. J. Real-Time Regulation of Catalysis by Remote-Controlled Enzyme-Conjugated Gold Nanorod Composites for Aldol Reaction-Based Applications. *Catal. Sci. Technol.* **2019**, *9*, 2221−2230.

(14) Tadepalli, S.; Yim, J.; Madireddi, K.; Luang, J. Y.; Naik, R. R.; Singamaneni, S. Gold Nanorod-Mediated Photothermal Enhancement of the Biocatalytic Activity of a Polymer-Encapsulated Enzyme. *Chem. Mater.* **2017**, *29*, 6308−6314.

(15) Tadepalli, S.; Yim, J.; Cao, S. S.; Wang, Z. Y.; Naik, R. R.; Singamaneni, S. Metal-Organic Framework Encapsulation for the Preservation and Photothermal Enhancement of Enzyme Activity. *Small* **2018**, *14*, 1702382.

(16) Yang, S. Y.; Yao, D. F.; Wang, Y. S.; Yang, W. T.; Zhang, B. B.; Wang, D. B. Enzyme-Triggered Self-Assembly of Gold Nanoparticles for Enhanced Retention Effects and Photothermal Therapy of Prostate Cancer. *Chem. Commun.* **2018**, *54*, 9841−9844.

(17) Khiavi, M. A.; Safary, A.; Aghanejad, A.; Barar, J.; Rasta, S. H.; Golchin, A.; Omidi, Y.; Somi, M. H. Enzyme-Conjugated Gold Nanoparticles for Combined Enzyme and Photothermal Therapy of Colon Cancer Cells. *Colloids Surf., A* **2019**, *572*, 333−344.

(18) Yang, K. K.; Liu, Y. J.; Wang, Y.; Ren, Q. L.; Guo, H. Y.; Matson, J. B.; Chen, X. Y.; Nie, Z. H. Enzyme-Induced in Vivo Assembly of Gold Nanoparticles for Imaging-Guided Synergistic Chemo-Photothermal Therapy of Tumor. *Biomaterials* **2019**, *223*, 119460.

(19) Barros, H. R.; López-Gallego, F.; Liz-Marzán, L. M. Light-Driven Catalytic Regulation of Enzymes at the Interface with Plasmonic Nanomaterials. *Biochemistry* **2020**, No. 0c00447.

(20) Nel, A. E.; Madler, L.; Velegol, D.; Xia, T.; Hoek, E. M. V.; Somasundaran, P.; Klaessig, F.; Castranova, V.; Thompson, M.

Understanding Biophysicochemical Interactions at the Nano-Bio Interface. *Nat. Mater.* **2009**, *8*, 543−557.
(21) Ansari, S. A.; Husain, Q. Potential Applications of Enzymes Immobilized on/in Nano Materials: A Review. *Biotechnol. Adv.* **2012**, *30*, 512−523.
(22) Breger, J. C.; Ancona, M. G.; Walper, S. A.; Oh, E.; Susumu, K.; Stewart, M. H.; Deschamps, J. R.; Medintz, I. L. Understanding How Nanoparticle Attachment Enhances Phosphotriesterase Kinetic Efficiency. *ACS Nano* **2015**, *9*, 8491−8503.
(23) Breger, J. C.; Oh, E.; Susumu, K.; Klein, W. P.; Walper, S. A.; Ancona, M. G.; Medintz, I. L. Nanoparticle Size Influences Localized Enzymatic Enhancement-A Case Study with Phosphotriesterase. *Bioconjugate Chem.* **2019**, *30*, 2060−2074.
(24) de Barros, H. R.; Santos, M. C.; Barbosa, L. R. S.; Piovan, L.; Riegel-Vidotti, I. C. Physicochemical Study of the Interaction between Gold Nanoparticles and Lipase from Candida sp. (CALB): Insights into the Nano-Bio Interface. *J. Braz. Chem. Soc.* **2019**, *30*, 2231−2242.
(25) Kisukuri, C. M.; Palmeira, D. J.; Rodrigues, T. S.; Camargo, P. H. C.; Andrade, L. H. Bimetallic Nanoshells as Platforms for Metallo- and Biometallo-Catalytic Applications. *ChemCatChem* **2016**, *8*, 171−179.
(26) Wu, C. S.; Wu, C. T.; Yang, Y. S.; Ko, F. H. An Enzymatic Kinetics Investigation into the Significantly Enhanced Activity of Functionalized Gold Nanoparticles. *Chem. Commun.* **2008**, 5327−5329.
(27) Baumann, V.; Muhammed, M. A. H.; Blanch, A. J.; Dey, P.; Rodriguez-Fernandez, J. Biomolecules in Metal and Semiconductor Nanoparticle Growth. *Isr. J. Chem.* **2016**, *56*, 195−213.
(28) Johnson, B. J.; Algar, W. R.; Malanoski, A. P.; Ancona, M. G.; Medintz, I. L. Understanding Enzymatic Acceleration at Nanoparticle Interfaces: Approaches and Challenges. *Nano Today* **2014**, *9*, 102−131.
(29) Song, Y. H.; Chen, J. Y.; Liu, H. Y.; Song, Y. G.; Xu, F. G.; Tan, H. L.; Wang, L. Conformation, Bioactivity and Electrochemical Performance of Glucose Oxidase Immobilized on Surface of Gold Nanoparticles. *Electrochim. Acta* **2015**, *158*, 56−63.
(30) Lopez-Tobar, E.; Hernandez, B.; Ghomi, M.; Sanchez-Cortes, S. Stability of the Disulfide Bond in Cystine Adsorbed on Silver and Gold Nanoparticles As Evidenced by SERS Data. *J. Phys. Chem. C* **2013**, *117*, 1531−1537.
(31) Hakkinen, H. The Gold-Sulfur Interface at the Nanoscale. *Nat. Chem.* **2012**, *4*, 443−455.
(32) Irani, M.; Tornvall, U.; Genheden, S.; Larsen, M. W.; Hatti-Kaul, R.; Ryde, U. Amino Acid Oxidation of Candida antarctica Lipase B Studied by Molecular Dynamics Simulations and Site-Directed Mutagenesis. *Biochemistry* **2013**, *52*, 1280−1289.
(33) de Aberasturi, D. J.; Serrano-Montes, A. B.; Langer, J.; Henriksen-Lacey, M.; Parak, W. J.; Liz-Marzán, L. M. Surface Enhanced Raman Scattering Encoded Gold Nanostars for Multiplexed Cell Discrimination. *Chem. Mater.* **2016**, *28*, 6779−6790.
(34) Yuan, H. K.; Khoury, C. G.; Hwang, H.; Wilson, C. M.; Grant, G. A.; Vo-Dinh, T. Gold Nanostars: Surfactant-Free Synthesis, 3D Modelling, and Two-Photon Photoluminescence Imaging. *Nanotechnology* **2012**, *23*, 075102.
(35) Turkevich, J.; Stevenson, P. C.; Hillier, J. A Study of the Nucleation and Growth Processes in the Synthesis of Colloidal Gold. *Discuss. Faraday Soc.* **1951**, 55−75.
(36) Kheirolomoom, A.; Khorasheh, F.; Fazelinia, H. Influence of External Mass Transfer Limitation on Apparent Kinetic Parameters of Penicillin G Acylase Immobilized on Nonporous Ultrafine Silica Particles. *J. Biosci. Bioeng.* **2002**, *93*, 125−129.
(37) Kuttner, C.; Höller, R. P. M.; Quintanilla, M.; Schnepf, M. J.; Dulle, M.; Fery, A.; Liz-Marzán, L. M. SERS and Plasmonic Heating Efficiency from Anisotropic Core/Satellite Superstructures. *Nanoscale* **2019**, *11*, 17655−17663.
(38) Hendel, T.; Wuithschick, M.; Kettemann, F.; Birnbaum, A.; Rademann, K.; Polte, J. In Situ Determination of Colloidal Gold Concentrations with UV-Vis Spectroscopy: Limitations and Perspectives. *Anal. Chem.* **2014**, *86*, 11115−11124.
(39) Daniel, R. M.; Danson, M. J. Temperature and the Catalytic Activity of Enzymes: A Fresh Understanding. *FEBS Lett.* **2013**, *587*, 2738−2743.
(40) Rabbani, G.; Ahmad, E.; Khan, M. V.; Ashraf, M. T.; Bhat, R.; Khan, R. H. Impact of Structural Stability of Cold Adapted Candida antarctica Lipase B (CALB): In Relation to pH Chemical and Thermal Denaturation. *RSC Adv.* **2015**, *5*, 20115−20131.
(41) Armenia, I.; Bonavia, M. V. G.; De Matteis, L.; Ivanchenko, P.; Martra, G.; Gornati, R.; de la Fuente, J. M.; Bernardini, G. Enzyme Activation by Alternating Magnetic Field: Importance of the Bioconjugation Methodology. *J. Colloid Interface Sci.* **2019**, *537*, 615−628.
(42) Jain, P. K. Taking the Heat Off of Plasmonic Chemistry. *J. Phys. Chem. C* **2019**, *123*, 24347−24351.
(43) Chatterjee, H.; Rahman, D. S.; Sengupta, M.; Ghosh, S. K. Gold Nanostars in Plasmonic Photothermal Therapy: The Role of Tip Heads in the Thermoplasmonic Landscape. *J. Phys. Chem. C* **2018**, *122*, 13082−13094.
(44) Leitner, D. M.; Pandey, H. D.; Reid, K. M. Energy Transport across Interfaces in Biomolecular Systems. *J. Phys. Chem. B* **2019**, *123*, 9507−9524.
(45) Johnson, K. A. A Century of Enzyme Kinetic Analysis, 1913 to 2013. *FEBS Lett.* **2013**, *587*, 2753−2766.
(46) Powers, K. T.; Washington, M. T., *Analyzing the Catalytic Activities and Interactions of Eukaryotic Translesion Synthesis Polymerases*. 1st edition; Academic Press; 2017, 592.
(47) Hammes, G.; Hammes-Schiffer, S., *Physical Chemistry for the Biological Sciences*. 2nd edition; John Wiley & Sons: New Jersey, 2015; 55.
(48) Gadda, G.; Fitzpatrick, P. F. Solvent Isotope and Viscosity Effects on the Steady-State Kinetics of the Flavoprotein Nitroalkane Oxidase. *FEBS Lett.* **2013**, *587*, 2785−2789.
(49) Jaeger, K. E.; Dijkstra, B. W.; Reetz, M. T. Bacterial Biocatalysts: Molecular Biology, Three-Dimensional Structures, and Biotechnological Applications of Lipases. *Annu. Rev. Microbiol.* **1999**, *53*, 315−351.
(50) Telis, V. R. N.; Telis-Romero, J.; Mazzotti, H. B.; Gabas, A. L. Viscosity of Aqueous Carbohydrate Solutions at Different Temperatures and Concentrations. *Int. J. Food Prop.* **2007**, *10*, 185−195.
(51) Galmes, M. A.; Garcia-Junceda, E.; Swiderek, K.; Moliner, V. Exploring the Origin of Amidase Substrate Promiscuity in CALB by a Computational Approach. *ACS Catal.* **2020**, *10*, 1938−1946.
(52) Hoops, S.; Sahle, S.; Gauges, R.; Lee, C.; Pahle, J.; Simus, N.; Singhal, M.; Xu, L.; Mendes, P.; Kummer, U. COPASI-A COmplex PAthway SImulator. *Bioinformatics* **2006**, *22*, 3067−3074.
(53) Quinn, D. M. Solvent Isotope Effects for Lipoprotein-Lipase Catalyzed-Hydrolysis of Water-Soluble para-Nitrophenyl Esters. *Biochemistry* **2002**, *24*, 3144−3149.
(54) Bradford, M. M. Rapid and Sensitive Method for Quantitation of Microgram Quantities of Protein Utilizing Principle of Protein-Dye Binding. *Anal. Biochem.* **1976**, *72*, 248−254.
(55) Bastus, N. G.; Comenge, J.; Puntes, V. Kinetically Controlled Seeded Growth Synthesis of Citrate-Stabilized Gold Nanoparticles of up to 200 nm: Size Focusing versus Ostwald Ripening. *Langmuir* **2011**, *27*, 11098−11105.
(56) Johnson, K. A.; Goody, R. S. The Original Michaelis Constant: Translation of the Michaelis-Menten Paper. *Biochemistry* **2011**, *50*, 8264−8269.

https://dx.doi.org/10.1021/acscatal.0c04919
ACS Catal. 2021, 11, 414−423